IOP PUBLISHING JOURNAL OF PHYSICS: CONDENSED MATTER

J. Phys.: Condens. Matter **19** (2007) 463101 (30pp) doi:10.1088/0953-8984/19/46/463101

TOPICAL REVIEW

Mesoscale structures in microemulsions

S Komura

Department of Chemistry, Graduate School of Science and Engineering, Tokyo Metropolitan University, Tokyo 192-0397, Japan

E-mail: komura@tmu.ac.jp

Received 6 July 2007, in final form 6 September 2007
Published 23 October 2007
Online at stacks.iop.org/JPhysCM/19/463101

Abstract

Due to the existence of intermediate mesoscopic internal structures, soft matter exhibits various fascinating non-linear and non-equilibrium phenomena. In this review article, we focus on microemulsions consisting of water, oil, and surfactant from the viewpoint of soft matter physics. Microemulsions exhibit a rich phase behavior as the composition and/or the temperature is varied. In the middle phase, oil and water mix in the presence of surfactant molecules to form a mesoscopic bicontinuous structure. To explain the complex behavior of microemulsions, it is useful to employ phenomenological approaches such as the Ginzburg–Landau theory or the membrane theory. We discuss the Ginzburg–Landau theory and also review the Teubner–Strey model, the Gompper–Schick model, and the two-order-parameter model. Based on these models, we discuss the structure of the middle phase and its wetting transition. The membrane theory proposed by Helfrich is also useful for describing the physical properties of microemulsions. Various structures in microemulsions, such as droplets, bicontinuous and network structures, are properly accounted for by the curvature elasticity model. We focus on the Exxon model which clarifies the physical origin of the middle phase. Within the phenomenological level of description, we review the dynamical aspects of droplet and bicontinuous microemulsions. We also give an overview of microemulsions found in multicomponent polymeric systems (polymeric microemulsions). A discussion on recent applications of microemulsions completes the review.

Contents

1. Introduction 2
2. Microemulsions 3
   2.1. Interfacial tension 3
   2.2. Phase behavior 4
   2.3. Phase diagrams 5

3. Ginzburg–Landau theory 8
3.1. Teubner–Strey model 8
3.2. Structure of the middle phase 9
3.3. Gompper–Schick model 10
3.4. Wetting transition by the middle phase 11
3.5. Two-order-parameter model 12
4. Membrane approach 13
4.1. Curvature elasticity energy 13
4.2. Emulsification failure 13
4.3. Persistence length 15
4.4. Challenges to the bicontinuous structure 16
4.5. Exxon model 16
4.6. Origin of the middle phase 18
4.7. Network structure 19
5. Dynamics 20
5.1. Dynamics of microemulsion droplets 20
5.2. Dynamics of bicontinuous structure 22
6. Polymeric microemulsions 23
7. Recent applications of microemulsions 25
8. Conclusion 27
Acknowledgments 27
References 27

1. Introduction

When we try to mix oil and water, they separate into two phases by creating a horizontal interface between them. This everyday phenomenon occurs because the contact area between the oil and water is minimized due to the large interfacial tension acting between them (3–5×10^{-2} J m^{-2}). However, once we add surfactant molecules to such a binary system, the nature of the solution changes dramatically. A surfactant molecule contains both hydrophilic and hydrophobic parts. At the oil/water interface, surfactant molecules tend to orient themselves by pointing their hydrophilic part towards the water and hydrophobic part towards the oil. As a result, the effective interfacial tension decreases considerably. Thermodynamically stable solutions consisting of oil, water, and surfactant are called *microemulsions*. Microemulsions are almost transparent or light blue liquids. In contrast, milk and margarine which scatter light are called *macroemulsions*.

Microemulsions are an important subject of colloid science or surface science, and there are an enormous number of studies on them. From the viewpoint of applications, surfactants are used in the preparation of food, drugs, cosmetics and oil recovery systems. Detailed explanations of the subject are available in [1–3] and other textbooks on colloid chemistry [4]. It is not the purpose of this review article to cover all topics on microemulsions. Instead, I would like to give an overview of the physical and universal aspects of microemulsions.

Among the various physical approaches, phenomenological models are quite useful in soft matter physics. In such models, appropriate approximations are employed depending on the time and length scales of interest. Phenomenological approaches are universal on mesoscopic to macroscopic length and timescales. My main purpose here is to provide a concise review of the historically important phenomenological theories that describe mesoscale structures in microemulsions. Hence, I did not try to make a complete list of the references in this area, although I do cover the latest developments in this field as much as possible. It should be noted,

however, that phenomenological models explain only one relatively simple aspect of the rich and complex behaviors of such systems. There are various time and length scales involved, and these should be investigated with different experimental and theoretical approaches. By integrating all the knowledge obtained from various methods, one can draw a whole picture of microemulsions.

Before describing microemulsions, I should stress here the importance of mesoscale structures in soft matter. (General overviews of soft matter are available in text books [5–7] or in review articles [8–10].) Because the constituent molecules are relatively large, a mesoscopic internal structure spontaneously forms in typical soft matter such as polymers, liquid crystals, surfactants, or colloids. These structures play an essential role in determining the physical properties of the material. Examples of mesoscopic length scales (10–1000 nm) are the Flory radius of a polymer chain, the sizes of colloidal particles, bilayer vesicles, and microemulsion droplets. The pore sizes in aerosols and the domain sizes in microphase separated block copolymers also appear to be of the mesoscopic scale.

When the scale of the internal structure is L, the entropic modulus of the material is typically given by $G \sim k_{\mathrm{B}}T/L^3$, where k_{B} is the Boltzmann constant and T the temperature. (Note that G has dimensions of energy per unit volume.) For a typical solid, L corresponds to the atomic length scale, and the order of G ranges from 10^{10} to 10^{11} Pa at room temperature. On the other hand, for colloidal crystals, for example, particles are periodically arranged in space, and the typical distance between them is much larger than the atomic size. Hence the modulus of a colloidal crystal can be very small, e.g. 1–100 Pa, or 10^{10} times smaller than the modulus of ordinary solids.

The existence of mesoscopic length scales in soft matter is also reflected in the dynamical properties. If we regard the time needed to diffuse through the distance between the particles τ as a typical timescale of the system, we have $\tau \sim L^2/D$, where D is the particle diffusion constant. For simple liquids τ is about 10^{-12} s, i.e. the particle motion relaxes immediately. For colloidal crystals as well as other soft matter, τ ranges from 10^{-3} to 1 s, which is extremely slow. Hence, the mesoscopic length scale in soft matter leads to dramatic structural changes under weak external fields accompanied by a long relaxation time. This is why non-linear and non-equilibrium properties are significant in soft matter. However, there are important unresolved problems when dealing with the equilibrium properties of soft matter. Although this review mainly concerns microemulsions in equilibrium, it does provide some discussions on time-dependent phenomena.

In the next section, we discuss the basic properties of microemulsions, e.g. the interfacial tension and the phase behavior. Section 3 describes various Ginzburg–Landau theories that capture the essential features of microemulsions. Among these models, the Teubner–Strey model and its extensions are discussed in some detail. In section 4, we review membrane theory, which is based on the notion of curvature elasticity. After that, we introduce the Exxon model which can describe the phase behavior of microemulsions. Section 5 describes the dynamics of droplet and bicontinuous microemulsions. Section 6 briefly explains microemulsions found in polymeric systems, i.e. polymeric microemulsions. Finally, section 7 provides recent applications of mesoscale structures in microemulsions.

2. Microemulsions

2.1. Interfacial tension

As mentioned in the previous section, a microemulsion is a thermodynamically stable ternary solution made of water, oil, and surfactant. Hydrophilic and hydrophobic parts coexist in

a surfactant molecule. Adsorption of such molecules to an oil/water interface considerably decreases its interfacial tension. Below we explain why adsorption of surfactants reduces the interfacial tension.

For simplicity, consider an insoluble surfactant which dissolves neither in oil nor in water. If we add such surfactant molecules to a mixture of oil and water, they adsorb at the oil/water interface, and the area per surfactant molecule Σ decreases. However, since the interfaces cannot adsorb an infinite amount of surfactant, Σ will saturate at a certain value Σ^*. What happens if we further increase the amount of surfactant ? In order to incorporate more surfactant while keeping $\Sigma \approx \Sigma^*$, the oil and water form a complicated inter-connected structure so that there is a gain in the interfacial area. The interface characterized by $\Sigma \approx \Sigma^*$ is called the *saturated interface* [11].

We can express such a saturated state in terms of the free energy [12]. The free energy per surfactant molecule in the adsorbed monolayer $f_a(\Sigma)$ is written as

$$f_a(\Sigma) = \sigma_{ow}\Sigma + f_s(\Sigma), \tag{1}$$

where σ_{ow} is the oil/water interfacial tension, and $f_s(\Sigma)$ represents the interaction among the surfactant molecules. The effective interfacial tension is given by

$$\sigma(\Sigma) \equiv \frac{\partial f_a(\Sigma)}{\partial \Sigma} = \sigma_{ow} + \frac{\partial f_s(\Sigma)}{\partial \Sigma} = \sigma_{ow} - \Pi(\Sigma), \tag{2}$$

where $\Pi = -\partial f_s/\partial\Sigma$ is the surface pressure. Since $f_a(\Sigma)$ is minimized when $\Sigma = \Sigma^*$ for saturated interfaces, we have $\sigma(\Sigma = \Sigma^*) = 0$. In other words, the effective interfacial tension vanishes for a saturated interface. Hence, the interfacial tension is zero in the ideal case.

2.2. Phase behavior

By changing the temperature or the composition, microemulsions can be made to exhibit a rich phase behavior. As depicted in figure 1, three different types of phase separation take place in microemulsions. Figure 1(a) shows an O/W (oil-in-water) microemulsion in which oil droplets of mesoscopic size are dispersed in water and form a *droplet phase*. Section 4 discusses what determines the size of the oil droplet. This droplet phase coexists with an excess oil phase O (almost pure oil that cannot dissolve in water), and the whole system is in a two-phase coexistence state. Such a coexistence state is called a Winsor I microemulsion. The interfacial tension between the two phases (O/W and O) is roughly $\sigma_{om} \sim 10^{-4}$ J m^{-2}, which is two orders of magnitude smaller than the oil/water interfacial tension σ_{ow}. The opposite situation occurs in the W/O (water-in-oil) microemulsion shown in figure 1(c). Here an inverted droplet phase coexists with an excess water phase, resulting in another type of the two-phase state called a Winsor II microemulsion.

When the hydrophilic and hydrophobic parts of the surfactant are of comparable size, or when its affinities for oil and water are balanced, the solution separates into three coexisting phases. Such a state is called a Winsor III microemulsion as shown figure 1(b). The intermediate phase due to the gravitational effect that is between excess oil and excess water is called the *middle phase*. In the middle phase, almost equal amounts of oil and water mix on the mesoscopic length scale through the creation of enormous numbers of interfaces saturated with surfactant. (In some references, the middle phase is called the '*microemulsion phase*'. In this article, we will use the term microemulsions to refer to any solution containing oil, water, and surfactant.) As the amount of surfactant increases, the middle phase expands so that the two excess phases vanish and a one-phase state appears. In this situation, phase separation does not take place while the oil and water mix completely on the mesoscopic scale. If we further increase the surfactant content, the self-assembling nature of amphiphilic molecules

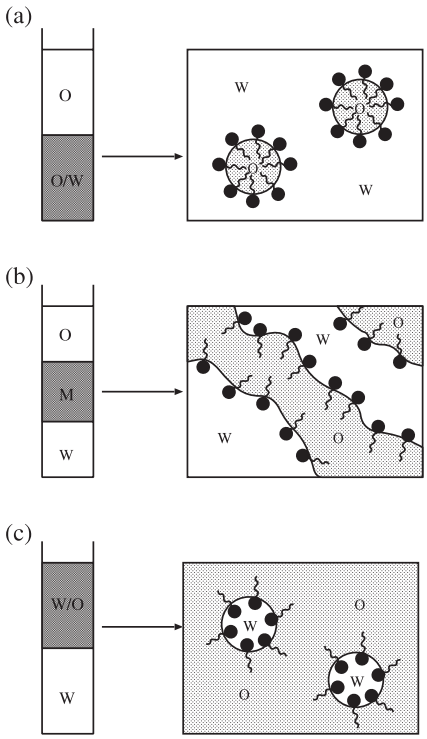

Figure 1. Phase separation and structures of microemulsions. A surfactant molecule has a hydrophilic head group and a hydrophobic tail group. (a) Oil-in-water (O/W) droplet phase coexisting with an excess oil (O) phase. The whole solution is in a two-phase coexistence state (Winsor I microemulsion). (b) Middle (M) phase coexisting with excess oil (O) and excess water (W) phases. A bicontinuous structure of oil and water domains separated by surfactant monolayers appears in the middle phase. The whole solution is in a three-phase coexistence state (Winsor III microemulsion). (c) Water-in-oil (W/O) droplet phase coexisting with an excess water (W) phase. The whole solution is in a two-phase coexistence state (Winsor II microemulsion).

induces liquid crystalline phases such as the *lamellar phase*, *hexagonal phase*, or *cubic phase*. All of these phases are characterized by spatially modulated ordered (rather than random) structures. The lamellar and hexagonal phases are analogous to the smectic and columnar phases in thermotropic liquid crystals [13].

2.3. Phase diagrams

The phase behavior of ternary systems can be summarized by using the Gibbs phase triangle. Figure 2, taken from [14], is the Gibbs triangle of a ternary system consisting of water, octane, and $C_{10}E_5$ (non-ionic surfactant) at 44.6 °C. In this phase diagram, '1', '2', and '3' indicate the one-phase, two-phase, and three-phase regions, respectively, and 'L_α' denotes the lamellar phase. In the two-phase region, the solution separates into two different compositions given by the end points of the straight lines, which are called 'tielines'. In the three-phase region, the system separates into three different compositions corresponding to the vertices of the shaded triangle. There is also a coexistence region between the one-phase state and the lamellar phase.

The Gibbs triangle of figure 2 is for a particular temperature. Figure 3 schematically illustrates how the phase behavior evolves as the temperature increases. Here the dotted lines

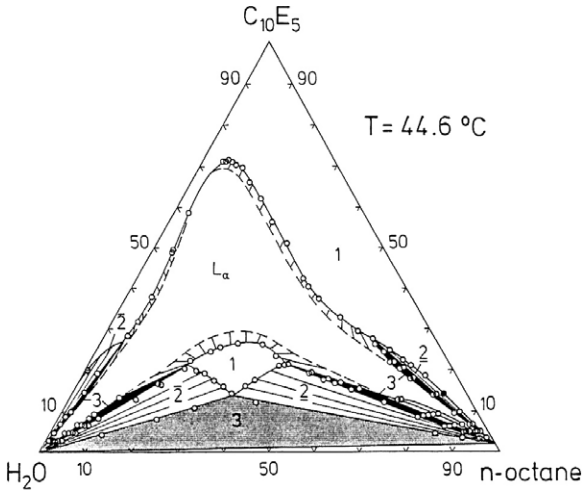

Figure 2. Gibbs triangle of a ternary microemulsion consisting of water, octane, and $C_{10}E_5$ (non-ionic surfactant) at 44.6 °C. '1', '2', and '3' indicate the one-phase, two-phase, and three-phase regions, respectively, and 'L_α' denotes the lamellar phase. Reprinted with permission from [14].

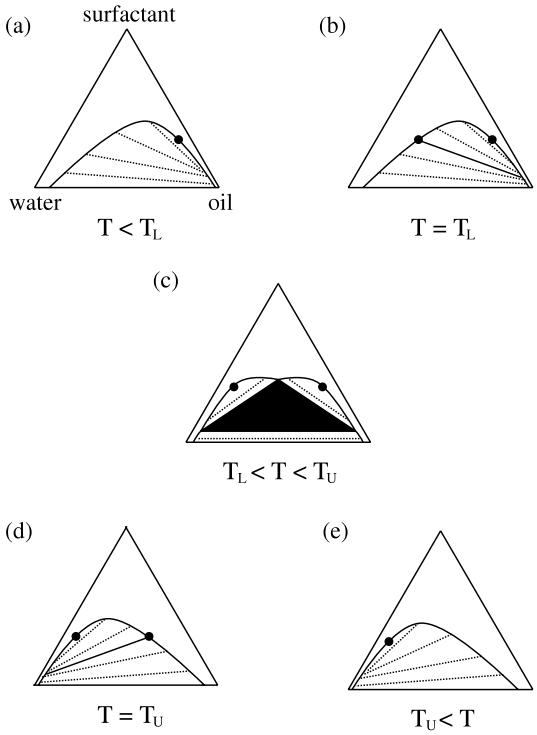

Figure 3. Temperature dependence of the Gibbs triangle for a ternary system consisting of oil, water, and surfactant. The temperature increases from (a) to (e). T_L and T_U correspond to the temperatures at the critical end points. A three-phase coexistence occurs in the temperature range $T_L < T < T_U$. The filled circles indicate the critical points.

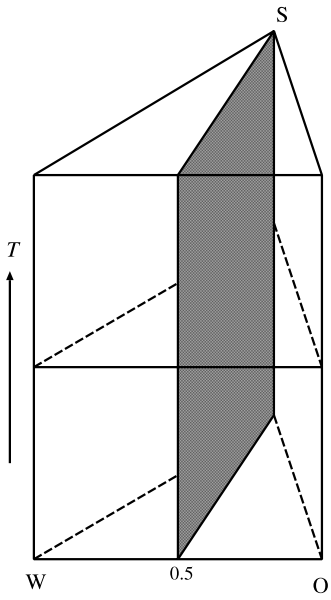

Figure 4. Phase prism of a ternary microemulsion consisting of oil (O), water (W), and surfactant (S). The vertical axis indicates temperature T. The shaded plane is a cut-through of the phase prism at a water-to-oil ratio of 1:1. On this plane, the horizontal axis is the surfactant concentration.

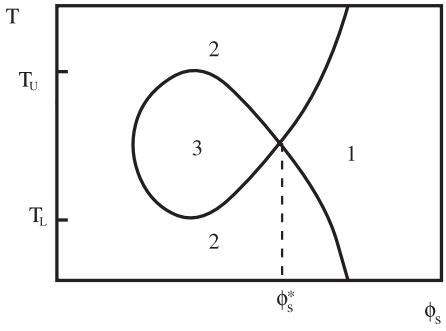

Figure 5. Phase diagram of temperature T versus surfactant concentration ϕ_s for a 1:1 water-to-oil ratio. This phase diagram corresponds to the shaded plane in figure 4. '1', '2', and '3' indicate the one-phase, two-phase, and three-phase regions, respectively.

represent the tielines, the shaded triangle corresponds to the three-phase region, and the filled circles are the critical points at which the two phases become identical (liquid crystalline phases are omitted). From this sequence of Gibbs triangles, we see that the three-phase coexistence (as depicted in figure 1(b)) only occurs when $T_L < T < T_U$. At either $T = T_L$ or $T = T_U$ corresponding to the *critical end points*, two of the three phases become identical so that the interface between them vanishes. For other temperatures, the solution is a two-phase coexistence state (figure 1(a) or (c)). By stacking a sequence of the Gibbs triangles along the temperature axis, one can construct a phase prism like the one shown in figure 4.

The shaded plane in figure 4 shows a cut-through of the phase prism at a 1:1 ratio of water to oil. The vertical and horizontal axes correspond to temperature and surfactant volume fraction, respectively. On this plane, the phase behavior is typically as in figure 5,

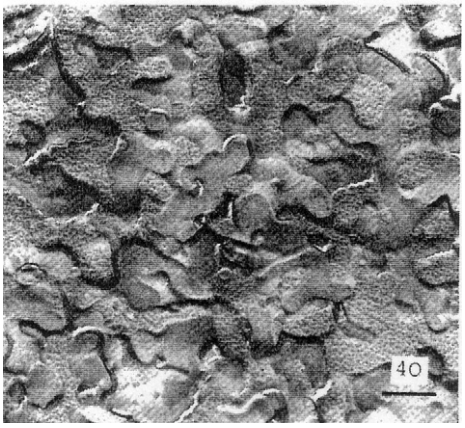

Figure 6. Freeze-fracture microscopy image of a microemulsion in the one-phase region (the middle phase). The scale bar indicates 200 nm. The structure is a bicontinuous one in which oil and water regions are randomly inter-connected. Reprinted with permission from [18].

which is called a 'fish' diagram according to the shape of the three-phase body. In this representation, one can easily see that the three-phase coexistence occurs only when $T_L < T < T_U$. A temperature-induced transition from an O/W microemulsion (figure 1(a)) to a W/O microemulsion (figure 1(c)) is called a *phase inversion*.

As stated before, oil and water mix in a single phase when the amount of surfactant is relatively large. The largest surfactant composition that forms the three-phase body in figure 5 is denoted as ϕ_s^*. In other words, ϕ_s^* is the minimum amount of surfactant required to mix oil and water in the one-phase state. In the applications of microemulsions, it is important to make ϕ_s^* as small as possible.

So far we have explained the phase behaviors and the phase diagrams of ternary microemulsions. In the following, we describe several phenomenological models that explain these interesting properties of microemulsions. Depending on the length scale, there are various approaches such as lattice spin models, Ginzburg–Landau models, and membrane theories. Here we shall mainly discuss the latter two approaches. Readers may find more complete descriptions in [15–17].

3. Ginzburg–Landau theory

3.1. Teubner–Strey model

Figure 6 shows a typical one-phase microemulsion structure (the middle phase) obtained from freeze-fracture microscopy [18]. We see that almost equal amounts of oil and water mix to form a sponge-like bicontinuous structure. The typical size of this bicontinuous structure is about 10–100 nm, which corresponds to the mesoscopic length scale. Why such a random bicontinuous structure is thermodynamically stable is an interesting question.

Small-angle x-ray or neutron scattering methods are useful to investigate such bicontinuous structures. Although microemulsions do not scatter light and look transparent, they do scatter x-rays and neutrons. Teubner and Strey suggested that the water–water structure function of the middle phase fits the following functional form [19, 20]:

$$S(\mathbf{q}) = \frac{aS(0)}{cq^4 + gq^2 + a}, \tag{3}$$

where **q** is the wavevector, q is its magnitude, and c, g, and a are the phenomenological parameters. In the middle phase, they satisfy $c > 0$, $a > 0$, and $g < 0$, but we also allow g to take on a positive value. The values of the parameters depend on the composition and/or the temperature.

When $g < 0$, the above structure function shows a peak at a non-zero wavevector

$$q^* = (-\gamma)^{1/2} \left(\frac{a}{c}\right)^{1/4}, \tag{4}$$

where $\gamma = g/\sqrt{4ac}$. Roughly speaking, this means the typical length scale of the structure in the middle phase is about $2\pi/q^*$. The fact that equation (3) decays as q^{-4} in the high-q limit is in accordance with Porod's law reflecting the existence of a large number of interfaces [21]. As the surfactant concentration increases and the water-to-oil ratio stays constant at 1:1, the peak position shifts to higher q so that the structure becomes smaller and the peak intensity decreases, meaning less contrast between oil and water [22].

Teubner and Strey proposed a free energy functional that reproduces the structure function (3). They chose the difference in the local volume fractions of oil and water as the order parameter $\psi(\mathbf{r})$. The suggested Ginzburg–Landau type of free energy functional is [19]

$$F_{\mathrm{TS}}[\psi(\mathbf{r})] = \int \mathrm{d}\mathbf{r}\,[c(\nabla^2\psi)^2 + g(\nabla\psi)^2 + a\psi^2]. \tag{5}$$

Notice that this free energy is invariant under the transformation $\psi \to -\psi$.

3.2. Structure of the middle phase

We will use the Teubner–Strey model to discuss the structure of the middle phase. The real-space water–water correlation function $G(\mathbf{r})$ can be obtained from the Fourier transform of equation (3). The correlation function $G(\mathbf{r})$ gives the probability of finding water at **r** given that water exists at the origin. When $-1 \leqslant \gamma \leqslant 1$, it has the following form:

$$G(\mathbf{r}) = \frac{\xi\lambda}{32\pi^2 cr}\, \mathrm{e}^{-r/\xi} \sin\frac{2\pi r}{\lambda}, \tag{6}$$

where the correlation length ξ is

$$\xi = \left(\frac{4c}{a}\right)^{1/4} \frac{1}{(1+\gamma)^{1/2}}, \tag{7}$$

and the characteristic wavelength λ is

$$\frac{\lambda}{2\pi} = \left(\frac{4c}{a}\right)^{1/4} \frac{1}{(1-\gamma)^{1/2}}. \tag{8}$$

Equation (6) is an oscillating function whose amplitude decays exponentially. This oscillation reflects the ability of surfactant to induce structural ordering between oil and water.

The dimensionless parameter γ measures the ability of the surfactant to form internal structures. Qualitatively speaking, the surfactant is 'stronger' when γ is negative and its absolute value is larger, whereas it is 'weaker' when γ becomes positive. If $\gamma > 1$, the correlation function becomes the Ornstein–Zernike form which decays monotonically, and no structure exists in the liquid. When $\gamma < -1$, the most stable structure is the periodic lamellar phase. Within the mean-field approximation in which we neglect thermal fluctuations, these behaviors can be summarized in the phase diagram shown in figure 7.

In figure 7, there are two distinct phases, i.e. disordered and lamellar. The second-order transition between these two phases occurs at $\gamma = -1$. The correlation function $G(\mathbf{r})$ has an oscillating component for $-1 \leqslant \gamma \leqslant 1$ (structured-disordered phase), whereas it decays

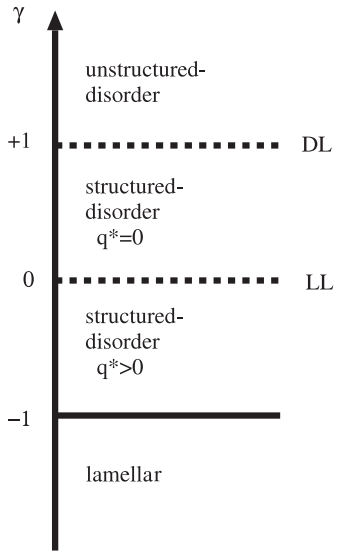

Figure 7. Phase diagram of the Teubner–Strey model in terms of $\gamma = g/\sqrt{4ac}$. DL at $\gamma = 1$ is the disorder line, and LL at $\gamma = 0$ is the Lifshitz line. The boundary between the lamellar and the disordered phases is at $\gamma = -1$. In the structured-disordered phase ($-1 < \gamma < 1$), the correlation function has an oscillating component, whereas in the unstructured-disordered phase ($\gamma > 1$), it decays monotonically. Inside the structured-disordered phase, the structure function has a peak at a finite wavevector $q^* > 0$ for $-1 < \gamma < 0$, and at $q^* = 0$ for $0 < \gamma < 1$.

monotonically for $\gamma > 1$ (unstructured-disordered phase). The line $\gamma = 1$ separating these structures is called the *disorder line* although it is not a phase boundary. The line $\gamma = 0$ (or $g = 0$) is the *Lifshitz line* at which q^* in equation (4) vanishes. When $0 \leqslant \gamma \leqslant 1$, $G(\mathbf{r})$ oscillates in space, but the structure function $S(\mathbf{q})$ does not show any peak. This means the surfactant is relatively weak. A peak appears in $S(\mathbf{q})$ when $-1 \leqslant \gamma \leqslant 0$, indicating a well developed structure in the middle phase.

3.3. Gompper–Schick model

The free energy (5) describes the structure of the middle phase, but it can only deal with a one-phase state. To consider a multi-phase coexistence, Gompper and Schick extended the Teubner–Strey model in the following way [23].

First, the term $a\psi^2$ in equation (5) is replaced so that three-phase coexistence is possible. Unlike the middle phase, the excess water phase ($\psi > 0$) or the excess oil phase ($\psi < 0$) does not have a mesoscale structure. Hence, these two excess phases have a positive g because the peak of the structure function is at $q = 0$. In general, g can be a function of ψ. From these considerations, Gompper and Schick proposed the following free energy functional [23]:

$$F_{\mathrm{GS}}[\psi(\mathbf{r})] = \int \mathrm{d}\mathbf{r}\,[c(\nabla^2\psi)^2 + g(\psi)(\nabla\psi)^2 + f(\psi)], \tag{9}$$

where $f(\psi)$ and $g(\psi)$ are given, for example, by

$$f(\psi) = \begin{cases} \omega_2(\psi - \psi_{\mathrm{b}})^2 & \psi > \psi_0 \\ \omega_0\psi^2 & |\psi| < \psi_0 \\ \omega_2(\psi + \psi_{\mathrm{b}})^2 & \psi < -\psi_0 \end{cases} \tag{10}$$

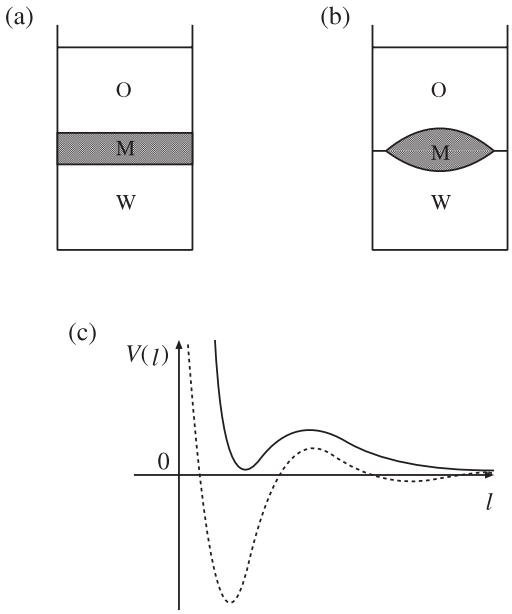

Figure 8. (a) The situation in which the middle phase wets the oil/water interface. (b) The situation in which the middle phase does not wet the oil/water interface and forms a lens. (c) Schematic representation of the interaction energy $V(\ell)$ between the oil/water interface. The dotted line is the result of the mean-field approximation; $V(\ell)$ is minimized at finite ℓ and hence the middle phase does not wet the interface. The solid line takes into account van der Waals interactions and/or thermal fluctuations; $V(\ell)$ is minimized when $\ell \to \infty$. In such a case, a macroscopically thick middle phase wets the oil/water interface.

and

$$g(\psi) = \begin{cases} b_0 & |\psi| < \psi_0 \\ b_2 & |\psi| > \psi_0. \end{cases} \tag{11}$$

Here, the constants are taken to be $b_0 < 0$ and $b_2 > 0$. The function $f(\psi)$ is continuous when $\psi_0 = \psi_b/(1 + \sqrt{\omega_0/\omega_2})$, and is minimized when $\psi = 0$ and $\pm\psi_b$. Using the above model, Gompper and Schick investigated interfacial profiles, elastic properties of interfaces, and phase behaviors of microemulsions. We refer the reader to [15] for their results.

3.4. Wetting transition by the middle phase

Here we briefly describe the wetting of the oil/water interface by the middle phase. This is an interesting phenomenon in which the structure of the middle phase affects the macroscopic behavior of the solution.

In section 2.2, we saw that the middle phase is located between the two excess phases. This means the oil/water interface is wet by the middle phase. Such a wetting phenomenon occurs for relatively short and weak (large γ) surfactants. For longer and stronger (small γ) surfactants, the middle phase does not wet the oil/water interface and forms a lens as depicted in figure 8. The transition from the non-wet state to the wet state is called the *wetting transition* [24].

To judge whether the oil/water interface is wet by the middle phase, we write the excess energy due to the interface as a function of the thickness of the middle phase ℓ;

$$\sigma(\ell) = \sigma_{wm} + \sigma_{om} + V(\ell). \tag{12}$$

Here, σ_{wm} and σ_{om} are the water/middle phase and oil/middle phase interfacial tensions, respectively, and $V(\ell)$ is the interaction potential between the interfaces. The effective oil/water interfacial tension σ_{ow} is determined from the minimum of $\sigma(\ell)$. If the minimum occurs at finite ℓ, the middle phase does not wet the oil/water interface. (A finite thickness is microscopic and the middle phase cannot form a macroscopic phase.) On the other hand, if $\sigma(\ell)$ takes a minimum value at infinite ℓ, then the interface will be wet by a macroscopically thick middle phase.

The interfacial properties are strongly dependent on the bulk properties. Using their model, Gompper and Schick showed that $V(\ell)$ is similar to equation (6), which is the product of an exponentially decaying function and an oscillating component [23]. A continuous wetting transition is expected at $\gamma = 1$ since the minimum of $V(\ell)$ continuously goes away to infinity as $\gamma \to 1$. (Notice that equation (8) diverges as $\gamma \to 1$.) As shown in figure 8(c), however, the minimum of $\sigma(\ell)$ always appears at finite ℓ as long as $-1 < \gamma < 1$. One might conclude that the middle phase never wets the oil/water interface. Such a conclusion contradicts the observed behavior in real microemulsions in which wetting indeed takes place.

To resolve this problem, we need to take into account the van der Waals interaction between the interfaces and also the steric interaction due to thermal fluctuations. The van der Waals interaction per unit area behaves roughly as $W\ell^{-2}$, where W is the Hamaker constant. Because the electron density of the middle phase takes an intermediate value between those of oil and water, $W\ell^{-2}$ is always positive. Therefore, the minimum of $V(\ell)$ at finite ℓ is shifted upward, as shown in figure 8(c), and the potential minimum goes away to $\ell \to \infty$.

Thermal fluctuation plays a similar role as van der Waals repulsion. It causes two interfaces (water/middle phase and oil/middle phase) to fluctuate; they collide with each other so that the allowed configurations are restricted. This reduces entropy and leads to a steric repulsive interaction. Thus, the same argument as above applies here. According to experiments using various surfactants, the middle phase that wets the interface is characterized not only by $\gamma < 1$ (below the disorder line) but also by $\gamma < 0$ (below the Lifshitz line) [25–27].

3.5. Two-order-parameter model

In the above Ginzburg–Landau model, the local volume fraction difference $\psi(\mathbf{r})$ between oil and water is chosen as the order parameter. According to the theory of critical phenomena, the coefficient a in equation (5) is proportional to the temperature difference $T - T_c$ measured from the critical temperature T_c. Since a is taken to be positive in the above models, the middle phase is expressed as a high-temperature disordered phase ($\psi = 0$). This means that within the single-order-parameter model, the local structure (or the separation between oil and water) of the middle phase is induced by thermal fluctuations.

A different approach is to introduce the surfactant concentration $\rho(\mathbf{r})$ and construct a two-order-parameter Ginzburg–Landau model using ψ and ρ [28, 29]. In this model, it is essential to consider the coupling between ψ and ρ. Since the free energy of the middle phase should be invariant under the transformation $\psi \to -\psi$, the possible coupling terms are such as $\rho\psi^2$, $\rho(\nabla\psi)^2$, and $(\nabla^2\rho)\psi^2$. For example, Komura and Kodama proposed the following model [29]:

$$F_{KK}[\psi(\mathbf{r}), \rho(\mathbf{r})] = \int d\mathbf{r}\,[c(\nabla^2\psi)^2 + g(\nabla\psi)^2 - a\psi^2 + u\psi^4 + e\rho^2(\rho - \rho_s)^2 - s\rho(\nabla\psi)^2], \tag{13}$$

where the phenomenological parameters c, g, a, u, e, s, and ρ_s are all taken to be positive. The last coupling term represents the fact that the surfactant adsorbs to the oil/water interface to lower its interfacial tension (represented by the coefficient of $(\nabla\psi)^2$). For saturated interfaces,

the parameters are chosen to satisfy $g = s\rho_s$. Since the coefficient of the ψ^2 term is negative in equation (13), the middle phase is a low-temperature one. Using this model, Kodama and Komura investigated the phase separation dynamics, or the rheology of the middle phase [30].

A vector nature of the surfactant molecule was taken into account in a different two-order-parameter model proposed by Chen *et al* [31].

4. Membrane approach

4.1. Curvature elasticity energy

Microemulsions can be described from a different point of view from that of the Ginzburg–Landau theory. As mentioned in section 2, surfactant molecules adsorb to oil/water interfaces to form monolayers which are in the fluid state. One can regard such a monolayer as a two-dimensional fluid whose thickness is negligibly small compared with its lateral size. Fluid membranes are very flexible and their configurations are characterized by the membrane curvature. Membrane theory is useful for describing large-scale phenomena such as the phase behavior of microemulsions.

Helfrich proposed the following curvature elasticity energy per unit area of the membrane [32]:

$$\begin{aligned} f_c(c_1, c_2) &= \tfrac{1}{2}\kappa(c_1 + c_2 - 2c_0)^2 + \bar{\kappa} c_1 c_2 \\ &= 2\kappa(H + c_0)^2 + \bar{\kappa} K, \end{aligned} \tag{14}$$

where c_1 and c_2 are the two principle curvatures. The combinations $H = -(c_1 + c_2)/2$ and[1] $K = c_1 c_2$ are the mean curvature and the Gaussian curvature, respectively. These quantities are the two invariants of a two-dimensional surface. The coefficients κ and $\bar{\kappa}$ are called the *bending modulus* and the *saddle-splay modulus*, respectively. Note that these moduli have the dimension of energy. While κ must always be positive because of the stability, $\bar{\kappa}$ can be both negative and positive. According to the Gauss–Bonnet theorem of differential geometry, the integral of the Gaussian curvature K over the whole surface is constant as long as the topology of the membrane is fixed.

The quantity c_0 is the *spontaneous curvature* that reflects the asymmetry between the inside and outside of the membrane. As we explain later, the phase inversion mentioned in section 2.3 occurs when c_0 changes sign. In the case of non-ionic surfactants, the spontaneous curvature vanishes at the temperature where the three-phase body meets the one-phase region (see figure 5). There are theories which relate the elastic moduli κ and $\bar{\kappa}$ to the phenomenological parameters c, g, and a of the Teubner–Strey model in equation (5) [33, 34].

4.2. Emulsification failure

We now discuss the relation between the curvature elasticity energy and the phase behavior of microemulsions [35]. Let the volume fractions of oil, water, and surfactant be ϕ_o, ϕ_w, and ϕ_s, respectively. Due to the incompressibility condition, these quantities amount to $\phi_o + \phi_w + \phi_s = 1$. For simplicity, we assume that all surfactant molecules adsorb to oil/water interfaces to form monolayers of a thickness δ that is almost equal to the surfactant size.

Consider a droplet phase in O/W microemulsions. We see below that the droplet size is uniquely determined by the average composition. We denote the radius of the spherical oil droplet by r, and the number of the oil droplets per unit volume by n. The following relations

[1] In some references, the mean curvature is defined as $H = +(c_1 + c_2)/2$, but according to differential geometry, it is more appropriate to define it with a negative sign.

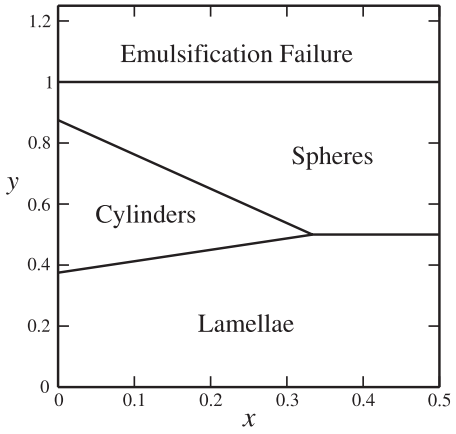

Figure 9. Phase diagram of various droplet structures based on the curvature elasticity model. The horizontal axis is $x = -\bar{\kappa}/(2\kappa + \bar{\kappa})$ and the vertical axis is $y = 3\tilde{c}_0\delta\phi_o/\phi_s$ (see the text). The droplet phase coexists with the excess oil phase in the 'emulsification failure' region.

hold from the incompressibility condition; $\phi_o = (4\pi/3)r^3 n$ and $\phi_s = 4\pi r^2 \delta n$. Hence, we have

$$r = \frac{3\delta\phi_o}{\phi_s}, \qquad n = \frac{\phi_s^3}{36\pi\delta^3\phi_o^2}. \tag{15}$$

On the other hand, if we put $c_1 = c_2 = c$ in equation (14) and minimize with respect to c, we obtain

$$\tilde{c}_0 = c_0\left(1 + \frac{\bar{\kappa}}{2\kappa}\right)^{-1}. \tag{16}$$

Notice that r is given by the composition of oil and surfactant, while $1/\tilde{c}_0$ is the material constant, and they generally differ. In the droplet phase, the competition between the two length scales (r and $1/\tilde{c}_0$) determines the phase behavior.

When the amount of surfactant is large so that $\tilde{c}_0 r < 1$, the system is in a one-phase state forming the droplet phase. In this situation, the droplet size decreases and the droplet number increases as ϕ_s becomes larger. However, when ϕ_s is small enough so that $\tilde{c}_0 r > 1$, some of the oil cannot be incorporated in the droplets and exists as an excess phase. This results in macroscopic phase separation, which is called *emulsification failure*. When this occurs, the droplet size is always given by $1/\tilde{c}_0$ which minimizes equation (14). Emulsification failure occurs when $\tilde{c}_0 r \approx 1$.

So far, we have considered spherical droplets, yet they can be also cylindrical or flat (lamellar). The radius of a cylindrical droplet is given by $2\delta\phi_o/\phi_s$. The (dimensionless) curvature energies per unit area of spherical (f_{sph}), cylindrical (f_{cyl}), and flat structures (f_{lam}) are respectively given by

$$\frac{f_{sph}}{2\tilde{\kappa}\tilde{c}_0^2} = \frac{1}{y^2} - \frac{2}{y}, \tag{17}$$

$$\frac{f_{cyl}}{2\tilde{\kappa}\tilde{c}_0^2} = \frac{9}{16y^2}(1 + x) - \frac{3}{2y}, \tag{18}$$

and f_{lam} =0, where $\tilde{\kappa} = \kappa + \bar{\kappa}/2$, $x = -\bar{\kappa}/2\tilde{\kappa}$, and $y = \tilde{c}_0 r$. By comparing these energies, we obtain the phase diagram shown in figure 9 [35].

The cylindrical structure appears when the absolute value of the negative saddle-splay modulus $\bar{\kappa}$ is small, i.e. $x < 1/3$. As x becomes larger, only the spherical and lamellar structures exist. The lamellar structure is more stable when $\tilde{c}_0$ is smaller. When $x = 0$ (or $\bar{\kappa} = 0$), the energies of the spherical and cylindrical droplets are degenerate. This means that spheres and cylinders coexist at $x = 0$.

The discussion up to now is correct when thermal fluctuations are negligible compared with the curvature energy. Since the entropic effect stabilizes small objects, the region of the spherical droplet expands when the entropy of mixing is taken into account. The effect of thermal fluctuations is discussed in [36]. Moreover, the above theory has been generalized to include translational entropy, cylinder length polydispersity, and radial polydispersity [37]. Recently, an analogy between emulsification failure and Bose–Einstein condensation has been proposed [38, 39].

4.3. Persistence length

Various experiments indicate that the bending modulus of a monolayer is of the order of several k_BT. Hence, the membrane's shape may be strongly affected by thermal fluctuations. As a quantity characterizing the membrane undulation due to thermal fluctuations, the so-called *persistence length* can be introduced [40], i.e.

$$\xi_\kappa \approx a \exp\left(\frac{4\pi\kappa}{\alpha k_B T}\right). \tag{19}$$

Here a is a microscopic length scale, and we assume $\alpha = 1$ in the following discussion. On a length scale larger than ξ_κ, the correlation in the membrane normal direction is completely lost and the membrane takes on a random configuration. On the other hand, the membrane can be regarded as statistically flat on a small length scale.

For a length scale comparable to ξ_κ, the curvature energy competes with the configurational entropy of the membrane. The effect of thermal fluctuations can be expressed in terms of a size-dependent effective bending modulus. For a membrane of size L, the renormalized bending modulus is [17, 41, 42][2]

$$\kappa_{\rm eff}(L) = \kappa\left[1 - \frac{k_BT}{4\pi\kappa}\log(L/a)\right]. \tag{20}$$

This formula states that the large-scale bending modulus is reduced due to thermal fluctuations[3]. The effective bending modulus $\kappa_{\rm eff}$ vanishes when the membrane size L becomes comparable to the persistence length ξ_κ. In this limit, there is no energy cost for bending.

Hereafter, we consider a 'balanced' microemulsion in which the amounts of oil and water are almost the same ($\phi_o \approx \phi_w$) and the spontaneous curvature is close to zero ($c_0 \approx 0$). We expect that the lamellar phase will appear in the absence of thermal fluctuations since a flat membrane ($c_1 = c_2 = 0$) minimizes the curvature energy. In reality, however, a random bicontinuous structure appears instead of the lamellar phase when ϕ_s is relatively small (see figures 5 and 6).

The existence of the bicontinuous structure can be qualitatively understood from the notion of persistence length [40]. In the lamellar phase, the distance between the monolayers d_L is determined by the average composition $d_L = \delta\phi_o/\phi_s \approx \delta/2\phi_s$ when $\phi_o \approx \phi_w \approx 1/2 \gg \phi_s$. Following the argument for the droplet phase, the competition between the lamellar structure

[2] The coefficients of $k_BT/(4\pi\kappa)$ in [41] and [42] are different. However, this difference is not essential in the following discussion.

[3] The saddle-splay modulus $\bar{\kappa}$ is also affected by thermal fluctuations. The length $\xi_{\bar{\kappa}}$ for which $\bar{\kappa}$ vanishes corresponds to the 'topological' persistence length [43–45].

and the random bicontinuous structure is determined by the ratio ξ_κ/d_L. The lamellar phase is stabilized when $\xi_\kappa > d_L$, whereas the random structure appears when $\xi_\kappa < d_L$ because the membranes fluctuate to gain entropy. This is why a random bicontinuous structure is observed at the tail of the 'fish' diagram (see figure 5).

Why does the three-phase body appear instead of the one-phase bicontinuous structure as the surfactant amount decreases? This question is intimately related to the physical origin of the middle phase. In the next subsections, we shall review some approaches to this problem.

4.4. Challenges to the bicontinuous structure

Talmon and Prager were the first to consider the bicontinuous structure of the middle phase [46]. In their picture, the whole space is divided into random Voronoi polyhedra, each filled with either oil or water. All the surfactant molecules are assumed to adsorb to the flat interfaces between oil and water. Their model takes into account the entropy of mixing between oil and water. However, it does not consider the curvature energy of the membrane.

Jouffroy *et al* improved the Talmon–Prager model in the following way [12]. Instead of dividing the space into Voronoi polyhedra, they considered cubic cells whose lattice constant is determined by the persistence length ξ_κ. They allow the area per surfactant Σ to fluctuate around Σ^*. Furthermore, they considered the curvature energy by choosing the local radius of curvature to be ξ_κ. This model successfully explains the two-phase coexistence but cannot obtain the three-phase coexistence, because the cell size is fixed to the persistence length ξ_κ.

Widom proposed a different model in which the size of the cubic cell is variable and is determined in a self-consistent manner at each point on the phase diagram [47]. The surfactant monolayers are assumed to form a compressible two-dimensional fluid in which the area per surfactant Σ can vary significantly. However, this assumption is contradictory to what happens at a saturated interface for which the area per surfactant is almost fixed to $\Sigma = \Sigma^*$. Nevertheless, Widom could obtain the three-phase coexistence by introducing a microscopic cutoff. He also concluded that the typical scale of the structure in the middle phase is of the order of 10 nm. However, this length scale has nothing to do with the persistence length. Hence, there was a problem in the Widom's model whereby the variation of the phase diagram due to the change in κ could not be reproduced.

4.5. Exxon model

Based on the above historical models, Safran and his group at Exxon Research and Engineering proposed the following model [48–50]. As depicted in figure 10, they divide the space into cubic cells whose size is d. Each cell is assumed to be occupied by either oil or water, and the surfactant molecules adsorb to the interfaces. Half of the surfactant volume fraction is assigned to oil and water volume fractions, i.e. $\phi = \phi_w + \phi_s/2$.

The first important aspect of the Exxon model is that the cell size d is not determined by the persistence length, but by the average composition of oil, water, and surfactant. The interface is assumed to be saturated so that the area per surfactant is constant, i.e. $\Sigma = \Sigma^*$. Given this condition and using a random mixing approximation, the cell size can be determined as

$$d = 6\delta \frac{\phi(1-\phi)}{\phi_s}. \tag{21}$$

The free energy (per unit volume) of mixing between oil and water is given by

$$f_{mix} = \frac{k_B T}{d^3} [\phi \log \phi + (1-\phi)\log(1-\phi)]. \tag{22}$$

Note that $1/d^3$ is the number of cells per unit volume.

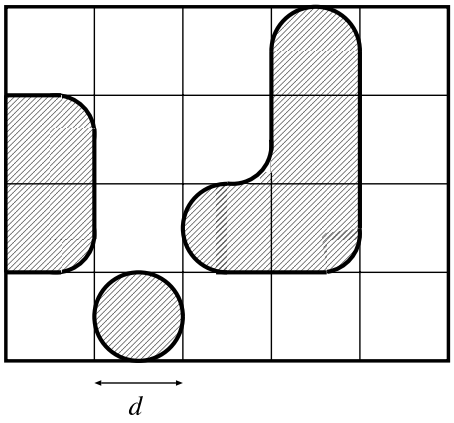

Figure 10. Model of the middle phase with a random bicontinuous structure. The three-dimensional space is divided into cubic cells of size d as given by equation (21). The shaded regions correspond to oil, the thick solid lines represent surfactant, and the rest is water.

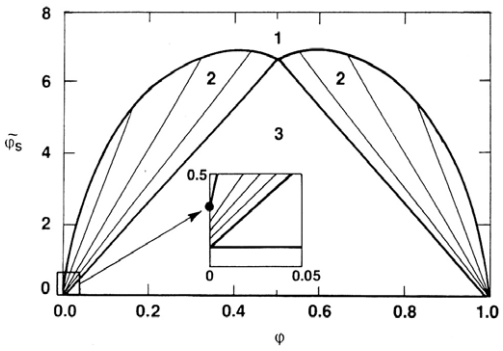

Figure 11. Phase diagram obtained from the Exxon model. The horizontal axis is the oil concentration, and the vertical axis $\tilde{\phi}_s = \phi_s \exp(1/t)$ represents the modified surfactant concentration. The parameters are $c_0 = 0$ and $t = 0.2$. The small ϕ region is magnified in the inset. The filled circle represents the critical point. Reprinted with permission from [48].

On the other hand, the curvature energy per unit volume is estimated as[4]

$$f_{\rm curv} = \frac{8\pi\kappa_{\rm eff}(d)}{d^3}\,\phi(1-\phi)[1 - c_0 d(1-2\phi)]. \tag{23}$$

The second important aspect of the Exxon model is that the effective bending modulus $\kappa_{\rm eff}(d)$ is used for the curvature energy. In terms of the persistence length ξ_κ, we can write $\kappa_{\rm eff}(d) = -t\kappa \log(d/\xi_\kappa)$, where $t = k_{\rm B}T/4\pi\kappa$ is the dimensionless temperature. The sum of equations (22) and (23) is the total energy per unit volume.

A typical phase diagram for $c_0 = 0$ and $t = 0.2$ is shown in figure 11. (The horizontal axis is ϕ and the vertical axis is $\tilde{\phi}_s = \phi_s \exp(1/t)$.) Here, all types of coexistence are reproduced in accordance with the phase behavior described in section 2.3. The inset shows the tielines in the small ϕ region, and the filled circle indicates the critical point.

Figure 12 shows the phase diagram for equal volume fractions of oil and water ($\phi_o = \phi_w$). Here, the horizontal axis is surfactant concentration $\tilde{\phi}_s$, and the vertical axis is dimensionless

[4] The factor 8π comes from the approximation that the membrane is regarded as a part of a sphere of radius $d/2$. The product $\phi(1-\phi)$ is proportional to the total area of the oil/water interface.

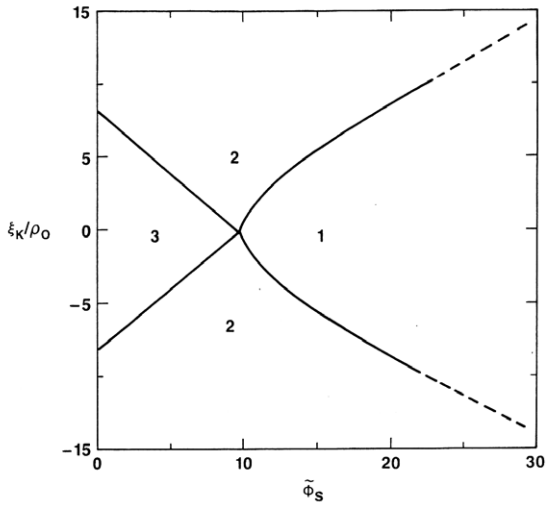

Figure 12. Phase diagram obtained from the Exxon model when the volume fractions of oil and water are equal. The horizontal axis $\tilde{\phi}_s = \phi_s \exp(1/t)$ is the surfactant concentration, and the vertical axis is the spontaneous curvature c_0 scaled by the persistence length ξ_κ. The temperature parameter is $t = 0.151$. Reprinted with permission from [50].

spontaneous curvature (the dimensionless temperature is $t = 0.151$) [50]. This phase diagram is analogous to the 'fish' diagram in figure 5 if the spontaneous curvature is a smooth function of temperature [51]. One can confirm that the spontaneous curvature vanishes when the three-phase body meets the one-phase region.

4.6. Origin of the middle phase

Here, we briefly discuss why the Exxon model can describe the three-phase coexistence state. Had we used a constant bending modulus κ instead of $\kappa_{\rm eff}(d)$ in equation (23), the total energy would scale as $f_{\rm mix} + f_{\rm curv} \sim \phi_s^3$ since $d \sim \phi_s^{-1}$. This scaling means that there is no characteristic length scale involved in the curvature energy [52]. We may conclude that the phase transition never occurs, no matter how much the surfactant volume fraction ϕ_s changes. However, the above contradiction disappears if equation (23) uses the effective bending modulus $\kappa_{\rm eff}(d)$, because the persistence length enters as a new length scale through $\kappa_{\rm eff}(d)$.

We mentioned before that the lamellar phase is stable when ϕ_s is large and $\xi_\kappa > d$, while the random structure is stable for the opposite conditions. Even if ϕ_s is very small, the one-phase state should in principle persist as long as d increases according to equation (21). As indicated by equation (22), however, the entropy dramatically decreases when d becomes large. Hence, the system prefers to be random at small length scales so that the excess oil and water separate macroscopically. When d becomes comparable to the persistence length ξ_κ, it is energetically unfavorable for the membranes to fluctuate at a smaller length scale because of the curvature energy. As a result of the balance between curvature energy and entropy, the bicontinuous structure in the middle phase becomes random on the length scale ξ_κ. However, it should be stressed that this fact is a consequence of the model, not of the assumption. Based on the Exxon model, the correlation and structure functions of microemulsions were calculated in [53]. An extension of the Exxon model is given in [54, 55].

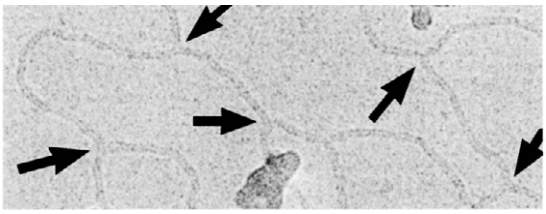

Figure 13. Transmission electron microscopy picture of a microemulsion in which an oil region has formed a network structure. Many Y-shaped junctions exist as indicated by the arrows. Reprinted with permission from [61].

In section 2.3, we defined the minimum surfactant volume fraction ϕ_s^* to mix oil and water. Since $d \approx \xi_\kappa$ at the boundary between the three-phase body and the one-phase region, we put $\phi \approx 1/2$ to obtain

$$\phi_s^* \approx \frac{3\delta}{2\xi_\kappa}. \tag{24}$$

Hence, ϕ_s^* is essentially inversely proportional to the persistence length ξ_κ.

After the Exxon model came out, Wennerström and Olsson proposed a simple free energy for balanced microemulsions based on the flexible membrane model [56]. In their model, the free energy per unit volume is given by

$$f_{\mathrm{WO}} = a_3\phi_s^3 + a_5\phi_s^5, \tag{25}$$

where a_3 can be negative and a_5 is positive for the reason of stability. The first term comes from the length scale invariance of the curvature energy, as discussed before. The above model can also explain three-phase coexistence when $a_3 < 0$ [57]. This model and the Exxon model were recently compared for balanced microemulsions [58].

4.7. Network structure

A bicontinuous structure appears when the spontaneous curvature is close to zero and the whole system is balanced. When the spontaneous curvature is large enough, we encounter droplet phases in which each globule is separated (see section 4.2). However, according to recent transmission electron microscopy experiments, the oil region forms a tubular network structure when the oil concentration is small [59]. Figure 13 is a picture of a network structure made of long tubes connected by Y-shaped junctions. To describe such a network structure, Tlusty *et al* proposed a model in which the competition between 'end caps' and 'junctions' of the tubes plays an essential role [60–62]. In the following, we explain their model briefly. A more extended treatment based on the spin model was given in [63].

First, we consider the network consisting of cylinders with different lengths. Let $c(m)$ be the number density of a cylinder of length m. (Here, the length of the cylinder is measured in units of its diameter and hence m is dimensionless.) If the inside of the cylinder is filled with oil, the volume conservation condition is

$$\phi_o = \int mc(m)\,\mathrm{d}m. \tag{26}$$

Since the number density of a z-folded junction ρ_z is $1/z$ times the number density of an isolated cylinder that has two end caps, it is given by

$$\rho_z = \frac{2}{z}\int c(m)\,\mathrm{d}m. \tag{27}$$

Here we fix z and consider the competition between the end caps of $z = 1$ and z-folded junctions.

By using these quantities, the free energy per unit volume can be written as [64]

$$\frac{f_n}{k_B T} = \int c(m)[\log c(m) - 1]\,dm + \rho_z \epsilon_z + (1 - z)\rho_z \log \rho_z, \tag{28}$$

where ϵ_z is the energy (divided by $k_B T$) required to form a single junction from z cylinders. The first term of equation (28) is the translational entropy of the free cylinders, and the second term corresponds to the curvature energy of the junctions. The last term represents the loss of the entropy when a single junction forms from z free end caps.

By minimizing the free energy (28) with respect to $c(m)$ under the constraint of (27), we obtain

$$c(m) \sim \exp(-2\epsilon_z/z)\, \rho_z^{2(1-1/z)}\, \exp(-m/M), \tag{29}$$

which is an exponentially decaying distribution function. Here, $M \sim \phi_o^{1-z/2} e^{\epsilon_z}$ and the coefficient of order unity is omitted. Substituting equation (29) into (28) yields the minimized free energy:

$$\frac{f_n}{k_B T} = -\rho_z \sim -\phi_o^{z/2} e^{-\epsilon_z}. \tag{30}$$

The above result has several interesting physical aspects. First, the junctions behave as an ideal gas since the free energy has the form $f_n \sim -k_B T \rho_z$. Second, the term $-\phi_o^{z/2} e^{-\epsilon_z}$ reflects an effective attraction between the oil molecules due to the presence of the junctions. In particular, the Y-shaped three-fold junction ($z = 3$) gives rise to a term $-\phi_o^{3/2} e^{-\epsilon_3}$. This term induces phase separation in the low ϕ_o limit by overcoming the repulsive excluded volume interaction term (proportional to $+\phi_o^2$). Accordingly, the phases of high and low density junctions coexist in equilibrium. A detailed analysis indicates that the coexistence region forms a closed loop [60].

Although a network structure forms when $z \geqslant 3$, the junctions of $z \geqslant 4$ seldom appear because of the Boltzmann factor $e^{-\epsilon_z}$. Hence it is enough to consider the competition between the end caps of $z = 1$ and the junctions of $z = 3$. The transition between the cylindrical structure and the network structure is determined by the condition $\rho_1 \simeq \rho_3$ or $\epsilon_3 - \epsilon_1 \simeq \log \phi_o$. Tlusty *et al* numerically estimated the curvature energies of the Y-shaped junction and the end cap to obtain the following relation [61, 62]:

$$\epsilon_3 - \epsilon_1 = 4\pi \frac{\kappa}{k_B T}(1.42 c_0 r - 1.04) - 4\pi \frac{\bar{\kappa}}{k_B T}, \tag{31}$$

where $r = 3\delta\phi_o/\phi_s$ is the radius of the spherical droplet[5].

As shown in figure 14, Tlusty *et al* were able to add a network structure to the phase diagram of figure 9 [61]. The network structure exists between the cylindrical and lamellar structures. Such a sequence of structural transitions is indeed observed in real microemulsions [59].

5. Dynamics

5.1. Dynamics of microemulsion droplets

The bending modulus κ and the saddle-splay modulus $\bar{\kappa}$ can be experimentally obtained from various scattering experiments that can resolve fluctuations of oil/water interfaces. Consider a

[5] Since r differs by a factor of 2/3 compared with that in [61], 1.42 in equation (31) is replaced with 2.14 in [61].

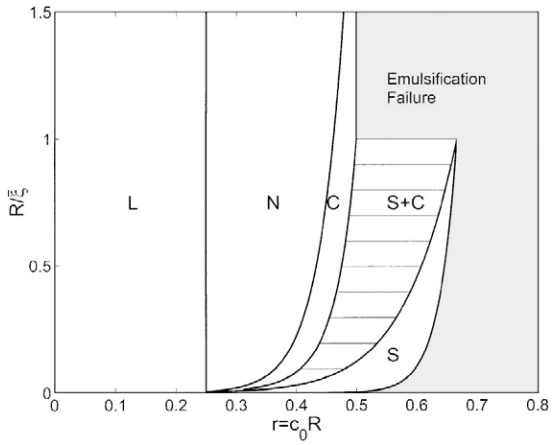

Figure 14. Phase diagram of a microemulsion obtained from the model of Tlusty *et al*. The horizontal axis is $2c_0\delta\phi_o/\phi_s$, and the vertical axis is $2\delta\phi_o/(\xi_\kappa\phi_s)$. S is the sphere, C the cylinder, N the network, and L the lamellar structure. S+C is the coexistence region between the spherical and cylindrical droplets. Reprinted with permission from [61].

spherical oil droplet of radius r_0. Let us denote the out-of-plane displacement of the membrane by $a(\theta, \varphi, t)$ depending on angles θ, φ and time t. It is convenient to expand $a(\theta, \varphi, t)$ in terms of spherical harmonics $Y_{lm}(\theta, \varphi)$:

$$a(\theta, \varphi, t) = \sum_{l,m} a_{lm}(t) Y_{lm}(\theta, \varphi). \tag{32}$$

Based on the curvature energy (14), Safran calculated the fluctuation amplitudes in thermal equilibrium to be [65–67]

$$\frac{\langle |a_{lm}|^2 \rangle}{r_0^2} = \frac{k_B T}{\kappa}\left[(l-1)(l+2)\left\{(l-2)(l+3) + 4c_0 r_0 - \frac{3\bar{\kappa}}{\kappa} - \frac{3k_B T}{4\pi\kappa} f(\phi)\right\}\right]^{-1}, \tag{33}$$

where

$$f(\phi) = \frac{1}{\phi}[\phi \log \phi + (1-\phi)\log(1-\phi)] \tag{34}$$

is the entropy of mixing per droplet.

In the presence of hydrodynamic flow, the membrane restoring force balances with the viscous resistance force due to the surrounding fluid after a short initial period of motion. In this case, the autocorrelation function of the out-of-plane displacement,

$$\langle a_{lm}(t) a_{l'm'}(0) \rangle = \delta_{ll'}\delta_{mm'} \langle |a_{lm}|^2 \rangle \exp(-t/\tau_{lm}) \tag{35}$$

decays exponentially with a relaxation time τ_{lm}. By employing the Stokes approximation for the hydrodynamic equations, several people have calculated the relaxation time under various conditions [66, 68, 69]. The most general form obtained by Seki and Komura is [70, 71]

$$\frac{1}{\tau_{lm}} = \frac{\kappa}{\eta r_0^3}\left[(l-2)(l+3) + 4c_0 r_0 - \frac{3\bar{\kappa}}{\kappa} - \frac{3k_B T}{4\pi\kappa} f(\phi)\right]\frac{1}{Z(l)}, \tag{36}$$

with

$$Z(l) = \frac{(l-1)(2l^2+5l+5)E + (l+2)(2l^2-l+2)}{(l-1)l(l+1)(l+2)}. \tag{37}$$

Here, $E = \eta'/\eta$ is the ratio of the viscosities of the interior and the continuous phase of the droplets. A somewhat similar calculation was performed by Lisy *et al* [72].

The situation becomes simpler when the droplet phase is in equilibrium with the excess oil phase. Then the droplets achieve their optimum size $r_0 = 1/\tilde{c}_0$, as given by equation (16). In the presence of the entropic term, one generally has

$$c_0 r_0 = 1 + \frac{\bar{\kappa}}{2\kappa} + \frac{k_B T}{8\pi\kappa} f(\phi), \tag{38}$$

instead of equation (16). By using this relation, we have the size polydispersity index p of the microemulsion droplet,

$$p^2 = \frac{\langle |a_{00}| \rangle}{4\pi r_0^2} = \frac{k_B T}{8\pi(2\kappa + \bar{\kappa}) + 2k_B T f(\phi)}, \tag{39}$$

and the relaxation time τ_2 for the 'peanut-like' deformation corresponding to the second-order spherical harmonic ($l = 2$),

$$\frac{1}{\tau_2} = \frac{1}{\eta r_0^3}\left[4\kappa - \bar{\kappa} - \frac{k_B T}{4\pi} f(\phi)\right]\frac{24}{32 + 23E}. \tag{40}$$

The relaxation time can be measured by neutron spin-echo (NSE) spectroscopy [73, 74]. This technique measures the correlation functions of the Brownian motions in a sample. On the other hand, the quantity p can be measured by small-angle neutron scattering (SANS) [75] or dynamic light scattering (DLS) [76, 77]. By using equations (39) and (40), the combination of NSE and either SANS or DLS enables us to determine the two elastic moduli [78]. For example, it was reported that $\kappa = 0.92 k_B T$ and $\bar{\kappa} = -0.38 k_B T$ for a system consisting of octane/water/$C_{10}E_5$ [76]. Such a combined technique has recently been used to measure the effect of pressure on the bending modulus [79, 80]. The dynamics of dense microemulsion droplets forming ordered cellular phases have also been investigated by NSE [81].

5.2. *Dynamics of bicontinuous structure*

So far we have discussed the deformation of spherical microemulsion droplets. Here we review some of the approaches to describe the dynamics of a bicontinuous structure. Milner *et al* suggested the existence of a mode associated with the formation and destruction of passages between different parts of oil and water networks [82]. Such a topological relaxation time is very long in phases with sharply defined interfaces and high activation energies. Experimentally, a long-time diffusive relaxation mode was found in microemulsions consisting of SDS, octanol, octane, and brine [83].

Gompper and Hennes calculated the dynamic structure function of microemulsions by using the time-dependent Ginzburg–Landau model [84, 85]. In the simplest case, the equation of motion for the order parameter $\psi(\mathbf{r}, t)$ (the difference between the oil and water volume fractions) can be written as

$$\frac{\partial \psi}{\partial t} = L\nabla^2 \frac{\delta F_{TS}}{\delta \psi}, \tag{41}$$

where F_{TS} is the Teubner–Strey free energy given by equation (5) and L is the Onsager coefficient. Notice that ψ is a conserved quantity. In this case, the dynamic correlation function is

$$S(\mathbf{q}, \omega) = \frac{2Lq^2}{\omega^2 + [2Lq^2(cq^4 + gq^2 + a)]^2}. \tag{42}$$

Gompper and Hennes conducted a field-theoretic study with a coupling to a hydrodynamic flow field, and showed that the correlation function oscillates in time [84]. Equation (41) was generalized to the case of a large number of components by Marconi and Corberi [86].

Later, Nonomura and Ohta used a variational approach to derive the equations of motion for microemulsions [87]. The hydrodynamic interaction acting in the bicontinuous structure is taken into account through the Oseen tensor. They showed that the intermediate structure function $S(\mathbf{q}, t)$ consists of two exponential functions:

$$\frac{S(\mathbf{q}, t)}{S(\mathbf{q})} = (1 - f)\mathrm{e}^{-\Gamma_{11}(q)t} + f\mathrm{e}^{-\Gamma_{22}(q)t}. \tag{43}$$

Here f is a small q-dependent constant, and the relaxation rate Γ_{11} contains the hydrodynamic effect. NSE measurements on microemulsions containing $C_{12}E_5$ [88, 89] and $C_{10}E_4$ [90] confirmed the validity of the above equation.

By extending equation (41), the rheology of bicontinuous microemulsions has been investigated as well. In the presence of a flow $\mathbf{v}$, the time evolution of the order parameter $\psi(\mathbf{r}, t)$ can be written as

$$\frac{\partial \psi}{\partial t} + \nabla \cdot (\psi \mathbf{v}) = L\nabla^2 \frac{\delta F_{\mathrm{TS}}}{\delta \psi}, \tag{44}$$

where the velocity field is governed by the Navier–Stokes equation. Such a model was first proposed by Pätzold and Dawson [91, 92]. Under a steady shear flow, Corberi *et al* predicted a shear thinning behavior of microemulsions [93, 94]. Later Rapapa and Maliehe calculated the dynamic structure function $S(\mathbf{q}, t)$ under the shear flow along the Lifshitz line [95]. They predicted that $S(\mathbf{q}, t)$ shows multiscaling behavior, i.e. the characteristic length scales as $t^{7/6}$ in the flow direction, and as $t^{1/6}$ in directions perpendicular to the flow.

The above Ginzburg–Landau approach is valid for the intermediate and low-q regimes, i.e. $q \lesssim q^*$ where $2\pi/q^*$ is the typical domain size (see equation (4)). For the high-q regime, $q \gtrsim q^*$, Zilman and Granek developed a theory in which microemulsion is treated as an ensemble of independent membranes with random orientations [96, 97]. The approximate expression for the intermediate structure function of an orientated membrane (in the z-direction) is a stretched exponential function

$$\frac{S(\mathbf{q}, t)}{S(\mathbf{q})} \approx \exp[-(\Gamma_{q_z} t)^{\beta}], \tag{45}$$

with $\beta = 2/3$ and the q_z-dependent relaxation rate is

$$\Gamma_{q_z} = 0.0246 \left(\frac{k_{\mathrm{B}}T}{\kappa}\right)^{1/2} \frac{k_{\mathrm{B}}T}{\eta} q_z^3. \tag{46}$$

To compare this equation with the experimental results, an average over all possible orientations of the membranes should be performed [96, 97]. The Zilman–Granek theory has been experimentally confirmed for microemulsions containing $C_{12}E_5$ by light scattering [98] and NSE [89].

6. Polymeric microemulsions

This section discusses microemulsions that have been found in polymeric systems. In these systems, diblock copolymers act as amphiphilic molecules. Various ordered structures form in pure diblock copolymer melts as a result of the microphase separation [99]. Recently, attention has focused on polymer mixtures that contain diblock copolymers and homopolymers. For example, in ternary mixtures consisting of AB block copolymer/A

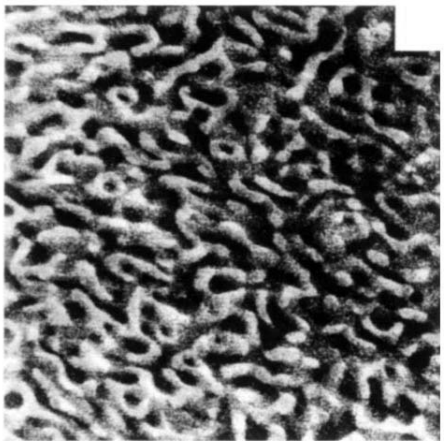

Figure 15. Transmission electron micrograph of a polymeric bicontinuous microemulsion consisting of symmetric PE-PEP/PE/PEP mixtures. Reprinted with permission from [100].

homopolymer/B homopolymer, the AB block copolymer adsorbs to the interface between the two homopolymers.

Similar to low molecular weight surfactants, there is a loss in mixing entropy when block copolymers adsorb to the interface. For diblock copolymer molecules, however, there is an additional loss in stretching entropy since the adsorbed molecules become elongated at the interface. Moreover, diblock copolymers spontaneously form various ordered structures by themselves, which do not occur for small surfactants. Although there are several differences between diblock copolymers and small surfactants, the mesoscale structures which are formed in polymeric ternary systems are analogous to those in ternary microemulsions consisting of oil/water/surfactant.

Some years ago, Bates *et al* found a random bicontinuous structure between the lamellar phase and the two-phase coexistence region in a polymeric ternary system [100–103]. The electron microscope picture in figure 15 is very similar to the bicontinuous structure observed in the low molecular weight microemulsion in figure 6. Hence, they called these structures *polymeric microemulsions*, and these have been found in several polymer mixtures. Concerning the physical origin of the polymeric microemulsions, Bates *et al* considered that the homopolymers swell the lamellar structure and thermal fluctuations destroy the lamellar order. There are theoretical predictions for efficient design of bicontinuous polymeric microemulsions [104, 105].

Thermal fluctuations do not have much effect on polymeric systems because each polymer consists of a large number of monomers. Hence, the properties of polymeric systems can be quantitatively described within a mean-field theory. In the self-consistent mean-field theory originally formulated by Edwards [106], the many-body problem is reduced to solve the configuration of a single chain in an external field. However, since this theory has difficulty in dealing with non-uniform systems, many approximations have been proposed over the past years. Recently, it became possible to solve the set of self-consistent equations numerically without using any approximation [107]. This method has been applied to polymeric ternary mixtures by Matsen to estimate the elastic properties of a diblock copolymer monolayer and the effective interaction between monolayers [108–110]. Also using self-consistent field theory, Kodama *et al* investigated the physical origin of polymeric microemulsions. They suggested that polymeric microemulsions are not induced by thermal fluctuations, but appear as a result of microphase sepa-

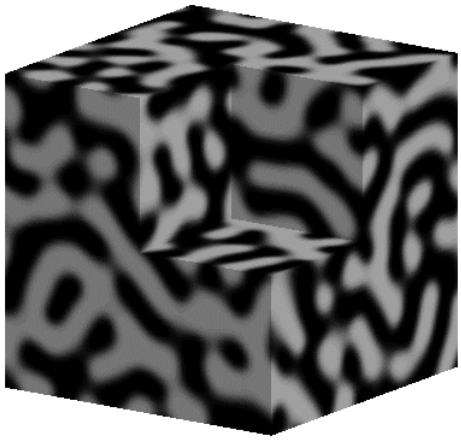

Figure 16. Bicontinuous structure calculated according to the real-space self-consistent field theory. Black and white regions correspond to A and B homopolymer rich regions, respectively.

ration without any structural order [111, 112]. Figure 16 shows the structure of a polymeric microemulsion obtained from a real-space calculation. A different approach to incorporate the effect of thermal fluctuations in field theory of ternary blends was proposed by Düchs *et al* [113].

The dynamic properties of polymeric bicontinuous microemulsions have recently attracted a lot of interest. For example, it was reported that shear flow transforms the microemulsion phase into a three-phase coexistence at strong shears, and it is followed by macrophase separation of homopolymers [114, 115]. For an intermediate shear rate, the viscosity shows shear thinning and the structure function is rendered anisotropic by the flow. The transient rheology [116] and linear viscoelasticity of polymeric microemulsions [117] have also been investigated. In the latter work, experimental data were compared with the theoretical predictions by Pätzold and Dawson [91, 92]. Using Brownian dynamics molecular simulations, Narayanan *et al* reproduced flow-induced phase transitions in ternary polymer blends [118]. Their results are in accord with the actual dynamical behavior of polymeric bicontinuous microemulsions [114, 115].

7. Recent applications of microemulsions

Let us review some of the recent applications of mesoscale structures in microemulsions.

(i) An interesting situation occurs when a small amount of amphiphilic diblock copolymer is added to a low molecular weight microemulsion. That is, there is a dramatic enhancement of the solubility between oil and water [119]. In figure 17, we show how the 'fish' phase diagram is modified in the presence of block copolymers. The addition of the amphiphilic block copolymer shifts the one-phase region to a smaller amphiphile volume fraction. Hence, the total volume fraction needed to form thermodynamically stable one-phase microemulsions is lower if a diblock copolymer/surfactant mixture is used instead of pure surfactant. Such a finding is very important and has been called the 'boosting effect'. Neutron scattering experiments demonstrated that the polymers form uniformly distributed mushroom conformations on the surfactant membrane [120–123].
This solubility phenomena can be attributed to the increase in the effective bending modulus caused by the addition of block copolymers. We should remind the reader that

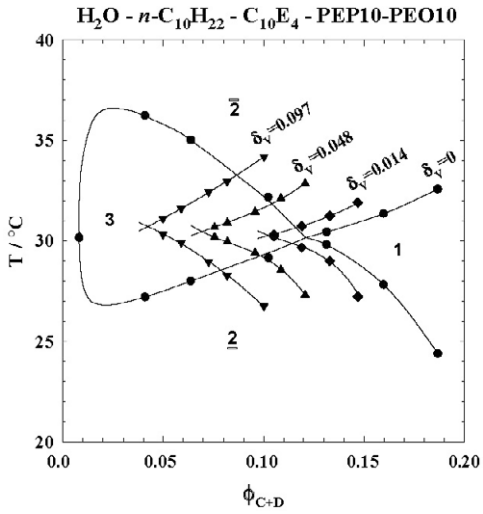

Figure 17. Three-phase body (3) and adjacent one-phase region (1) for water/*n*-decane/$C_{12}E_5$ containing equal volume fractions of oil and water. Addition of the amphiphilic block copolymer PEP10–PEO10 shifts the one-phase region to a smaller volume fraction ϕ_{C+D}. δ_v denotes the volume fraction of polymer in the surfactant. Reprinted with permission from [120].

according to equation (24), the minimum surfactant volume fraction needed to mix oil and water scales as $\phi_s^* \sim \xi_\kappa^{-1}$, where ξ_κ is the persistence length defined by equation (19). Hence, ϕ_s^* becomes smaller for a larger bending modulus. In the mushroom regime, the effect of polymer decoration on membrane elasticity is calculated to be [124]

$$\kappa_{\text{block}} = \kappa + \frac{k_B T}{12}\left(1 + \frac{\pi}{2}\right)\sigma(R_w^2 + R_o^2), \tag{47}$$

where σ is the number density of block copolymers within the membrane, and $R_{w/o}$ is the end-to-end distance of the hydrophilic/hydrophobic polymer block. The increase in bending modulus due to the polymers in the brush regime was calculated by Komura and Safran [125]. Later, dynamics of bicontinuous microemulsions with and without amphiphilic block copolymers were compared using NSE and DLS [126].

(ii) In contrast to amphiphilic block copolymers, the addition of two homopolymer chains diminishes the effect of the surfactant ('inverse boosting effect') [127]. In this case, a decrease in bending modulus was observed as homopolymer content increased. On the other hand, homopolymers increase the viscosities of oil and water. Dynamical measurements of the corresponding system revealed that the addition of homopolymer indeed reduces the bending modulus [128, 129].

(iii) Recently, Nakaya *et al* investigated the effect of confinement of water-soluble polymers inside spherical microemulsion droplets [130]. They showed that spherical droplets deformed to prolate ellipsoid droplets upon confinement, while keeping the total surface area and the volume of all the droplets constant. Increasing the degree of polymer confinement even further caused an isotropic–nematic transition in the concentrated droplet region. This result may be applicable to drug delivery.

(iv) It is known that systems composed of O/W microemulsion droplets linked by telechelic polymers form a multiconnected transient network [131]. Here, telechelic polymers have a hydrophilic backbone with a hydrophobic group at each chain end. These mixtures provide a wide range of technological applications such as cosmetics, paints, and oil

recovery. In such systems, the large one-phase region consists of a fluid sol phase and a viscoelastic gel phase separated by a percolation line. On the other hand, phase separation into a dilute sol phase and a concentrated gel phase occurs in the two-phase region [131]. The phase behavior and structure of microemulsion–telechelic mixtures was theoretically studied by Zilman *et al* [132]. Here the phase transition is driven by the competition between the translational entropy of the droplets and the configurational entropy of the polymer connections between them. The immunity of such a transient network to random degradation of the polymers has also been studied [133].

(v) Due to the presence of both polar and nonpolar solvents within the homogeneous continuum, microemulsions are often used as reaction media. For example, these systems are used for preparative organic synthesis and in bio-organic reactions such as lipase catalysed reactions. There have been many attempts to fix the mesoscale structures of the microemulsion through chemical reactions within the system. For instance, polymerization reactions can be used in microemulsions to produce analogs of latex particles [134]. Various other applications using reactions in microemulsions have been investigated in relation to catalysis, drug delivery, etc. Chemical reactions in microemulsions were theoretically studied by Ganesan and Fredrickson; they considered the effects of thermal fluctuations on reaction kinetics [135]. Fluctuations increase the reaction rate but do not affect the long-time dynamical evolution.

8. Conclusion

This review focused on microemulsions consisting of oil/water/surfactant and explained their mesoscale behaviors from the viewpoint of soft matter physics. Several phenomenological approaches turn out to be quite useful. For instance, the Ginzburg–Landau theories and membrane theories are universal. We also discussed polymeric microemulsions as a related system. It is quite surprising that the variety of mesoscale structures and macroscopic phase behaviors of microemulsions can be described by fairly simple models.

We limited the discussion to cases where the amount of surfactant is relatively small. Various liquid crystalline phases start to appear as the surfactant concentration increases. Microemulsions exhibit various delicate properties because they have characteristics of both liquids and liquid crystals. The structure, phase behavior, and dynamics of microemulsions are 'intermediate' between those of liquids and liquid crystals.

Acknowledgments

This work is supported by KAKENHI (Grant-in-Aid for Scientific Research) on Priority Areas 'Soft Matter Physics' and Grant No. 18540410 from the Ministry of Education, Culture, Sports, Science and Technology of Japan.

References

[1] Rosano H L and Clausse M (ed) 1987 *Microemulsion Systems* (New York: Dekker)
[2] Friberg S E and Bothorel P (ed) 1987 *Microemulsions: Structure and Dynamics* (Boca Raton, FL: CRC Press)
[3] Kumar P and Mittal K L (ed) 1999 *Handbook of Microemulsion Science and Technology* (New York: Dekker)
[4] Evans D F and Wennerström H 1994 *The Colloidal Domain* (New York: VCH)
[5] Hamley I W 2000 *Introduction to Soft Matter* (Chichester: Wiley)
[6] Jones R A 2002 *Soft Condensed Matter* (Oxford: Oxford University Press)

[7] Witten T A and Pincus P A 2004 *Structured Fluids: Polymers, Colloids, Surfactants* (Oxford: Oxford University Press)
[8] Witten T A 1999 *Rev. Mod. Phys.* **71** S367
[9] Gelbart W M and Ben-Shaul A 1999 *J. Phys. Chem.* **100** 13169
[10] Hołyst R 2005 *Soft Matter* **1** 329
[11] Schulman J and Montagne J 1961 *Ann. New York Acad. Sci.* **92** 366
[12] Jouffroy J, Levinson P and de Gennes P G 1982 *J. Physique* **43** 1241
[13] de Gennes P G and Prost J 1995 *The Physics of Liquid Crystals* (Oxford: Oxford University Press)
[14] Strey R 1993 *Ber. Bunsenges. Phys. Chem.* **97** 742
[15] Gompper G and Schick M 1994 *Self-Assembling Amphiphilic Systems* (San Diego, CA: Academic)
[16] Gelbart W M, Ben-Shaul A and Roux D (ed) 1994 *Micelles, Membranes, Microemulsions, and Monolayers* (New York: Springer)
[17] Safran S A 1994 *Statistical Thermodynamics of Surfaces, Interfaces, and Membranes* (New York: Addison-Wesley)
[18] Jahn W and Strey R 1988 *J. Phys. Chem.* **92** 2294
[19] Teubner M and Strey R 1987 *J. Chem. Phys.* **87** 3195
[20] Komura S, Seto H, Takeda T, Nagao M, Ito Y and Imai M 1996 *J. Chem. Phys.* **105** 3264
[21] Onuki A 1994 *Phase Transition Dynamics* (Cambridge: Cambridge University Press)
[22] Kotlarchyk M, Chen S-H, Huang J S and Kim M W 1984 *Phys. Rev. Lett.* **53** 941
[23] Gompper G and Schick M 1990 *Phys. Rev. Lett.* **65** 1116
[24] Schick M 1996 *Ber. Bunsenges. Phys. Chem.* **100** 272
[25] Schubert K-V and Strey R 1991 *J. Chem. Phys.* **95** 8532
[26] Schubert K-V, Strey R, Kline S R and Kaler E W 1994 *J. Chem. Phys.* **101** 5343
[27] Gradzielski M, Langevin D, Sottmann T and Strey R 1996 *J. Chem. Phys.* **104** 3782
[28] Laradji M, Guo H, Grant M and Zuckermann M J 1991 *J. Phys. A: Math. Gen.* **24** L629
[29] Komura S and Kodama H 1997 *Phys. Rev.* E **55** 1722
[30] Kodama H and Komura S 1997 *J. Physique* II **7** 74
[31] Chen K, Jayaprakash C, Pandit R and Wenzel W 1990 *Phys. Rev. Lett.* **65** 2736
[32] Helfrich W 1973 *Z. Naturf.* c **28** 693
[33] Teubner M 1991 *Europhys. Lett.* **403** 14
[34] Pieruschka P and Safran S A 1993 *Europhys. Lett.* **22** 625
[35] Safran S A, Turkevich L A and Pincus P A 1984 *J. Physique Lett.* **45** L69
[36] Safran S A 1983 *J. Chem. Phys.* **78** 2073
[37] Blokhuis E M and Sager W F C 2001 *J. Chem. Phys.* **115** 1073
[38] Sear R P and Cuesta J A 2001 *Europhys. Lett.* **55** 451
[39] Cuesta J A and Sear R P 2002 *Phys. Rev.* E **65** 031406
[40] de Gennes P G and Taupin C 1982 *J. Phys. Chem.* **86** 2294
[41] Helfrich W 1985 *J. Physique* **46** 1263
[42] Peliti L and Leibler S 1985 *Phys. Rev. Lett.* **54** 1690
[43] Golubović L 1994 *Phys. Rev.* A **50** R2419
[44] Morse D C 1994 *Phys. Rev.* E **50** R2423
[45] Gompper G and Kroll D M 1998 *Phys. Rev. Lett.* **81** 2284
[46] Talmon Y and Prager S 1978 *J. Chem. Phys.* **69** 2984
[47] Widom B 1984 *J. Chem. Phys.* **81** 1030
[48] Safran S A, Roux D, Cates M E and Andelman D 1986 *Phys. Rev. Lett.* **57** 491
[49] Andelman D, Cates M E, Roux D and Safran S A 1987 *J. Chem. Phys.* **87** 7229
[50] Cates M E, Andelman D, Safran S A and Roux D 1988 *Langmuir* **4** 802
[51] Vollmer D and Vollmer J 2001 *Eur. Phys. J.* E **4** 153
[52] Porte G, Appell J, Bassereau P and Marignan J 1989 *J. Physique* **50** 1335
[53] Milner S T, Safran S A, Andelman D, Cates M E and Roux D 1988 *J. Physique* **49** 1065
[54] Golubović L and Lubensky T C 1989 *Europhys. Lett.* **10** 513
[55] Golubović L and Lubensky T C 1990 *Phys. Rev.* A **41** 4343
[56] Wennerström H and Olsson U 1993 *Langmuir* **9** 365
[57] Daicic J, Olsson U and Wennerström H 1995 *Langmuir* **11** 2451
[58] Balogh J, Kaper H, Olsson U and Wennerström H 2006 *Phys. Rev.* E **73** 041506
[59] Bernheim-Grosswasser A, Tlusty T, Safran S A and Talmon Y 1999 *Langmuir* **15** 5448
[60] Tlusty T, Safran S A, Menes R and Strey R 1997 *Phys. Rev. Lett.* **78** 2616
[61] Tlusty T, Safran S A and Strey R 2000 *Phys. Rev. Lett.* **84** 1244

[62] Tlusty T and Safran S A 2000 *J. Phys.: Condens. Matter* **12** A253
[63] Zilman A G and Safran S A 2002 *Phys. Rev.* E **66** 051107
[64] Drye T J and Cates M E 1992 *J. Chem. Phys.* **96** 1367
[65] Safran S A 1983 *J. Chem. Phys.* **78** 2073
[66] Milner S T and Safran S A 1987 *Phys. Rev.* A **36** 4371
[67] Safran S A 1991 *Phys. Rev.* A **43** 2903
[68] Schneider M B, Jenkins J T and Webb W W 1984 *J. Physique* **45** 1457
[69] Komura S and Seki K 1993 *Physica* A **192** 27
[70] Seki K and Komura S 1995 *Physica* A **219** 253
[71] Komura S 1996 *Vesicles* (New York: Dekker) p 198
[72] Lisy V, Brutovsky B and Zatovsky A V 1998 *Phys. Rev.* E **58** 7598
[73] Huang J S, Milner S T, Farago B and Richter D 1987 *Phys. Rev. Lett.* **59** 2600
[74] Farago B, Richter D, Huang J S, Safran S A and Milner S T 1990 *Phys. Rev. Lett.* **65** 3348
[75] Gradzielski M, Langevin D and Farago B 1996 *Phys. Rev.* E **53** 3900
[76] Hellweg T and Langevin D 1998 *Phys. Rev.* E **57** 6825
[77] Hellweg T and Langevin D 1999 *Physica* A **264** 370
[78] Lisy V and Brutovsky B 2000 *Phys. Rev.* E **61** 4045
[79] Kawabata Y, Nagao M, Seto H, Komura S, Takeda T, Schwahan D, Yamada N L and Nobutou H 2004 *Phys. Rev. Lett.* **92** 056103
[80] Kawabata Y, Seto H, Nagao M and Takeda T 2007 *J. Chem. Phys.* **127** 044705
[81] Molle B, de Geyer A, Guillermo A and Farago B 2003 *Phys. Rev. Lett.* **90** 068305
[82] Milner S T, Cates M E and Roux D 1990 *J. Physique* **51** 2629
[83] Peter U, Roux D and Sood A K 2001 *Phys. Rev. Lett.* **86** 3340
[84] Gompper G and Hennes M 1994 *Phys. Rev. Lett.* **73** 1114
[85] Hennes M and Gompper G 1996 *Phys. Rev.* E **54** 3811
[86] Marconi U M B and Corberi F 1995 *Europhys. Lett.* **30** 349
[87] Nonomura M and Ohta T 1999 *J. Chem. Phys.* **110** 7516
[88] Komura S, Takeda T, Kawabata Y, Ghosh S K, Seto H and Nagao M 2001 *Eur. Phys. J.* E **5** 329
[89] Komura S, Takeda T, Kawabata Y, Ghosh S K, Seto H and Nagao M 2001 *Phys. Rev.* E **63** 041402
[90] Holderer O, Frielinghaus H, Monkenbusch M, Allgaier J, Richter D and Farago B 2007 *Eur. Phys. J.* E **22** 157
[91] Pätzold G and Dawson K 1996 *J. Chem. Phys.* **104** 5932
[92] Pätzold G and Dawson K 1996 *Phys. Rev.* E **54** 1669
[93] Corberi F, Gonnella G and Suppa D 2001 *Phys. Rev.* E **63** 040501
[94] Gonnella G and Ruggieri M 2002 *Phys. Rev.* E **66** 031506
[95] Rapapa N P and Maliehe N B 2004 *Eur. Phys. J.* B **42** 567
[96] Zilman A G and Granek R 1996 *Phys. Rev. Lett.* **77** 4788
[97] Zilman A G and Granek R 2002 *Chem. Phys.* **284** 195
[98] Freyssingeas E, Roux D and Nallet F 1997 *J. Physique* II **7** 913
[99] Bates F S and Fredrickson G H 1999 *Phys. Today* **52** 32
[100] Bates F S, Maurer W W, Lipic P M, Hillmyer M A, Almdal K, Mortensen K, Fredrickson G H and Lodge T P 1997 *Phys. Rev. Lett.* **79** 849
[101] Hillmyer M A, Maurer W W, Lodge T P, Bates F S and Almdal K 1999 *J. Phys. Chem.* B **103** 4814
[102] Washburn N R, Lodge T P and Bates F S 2000 *J. Phys. Chem.* B **104** 6987
[103] Morkved T L, Stepanek P, Krishnan K, Bates F S and Lodge T P 2001 *J. Chem. Phys.* **114** 7247
[104] Fredrickson G H and Bates S 1997 *J. Polym. Sci.* B **35** 2775
[105] Fredrickson G H and Bates S 1998 *Eur. Phys. J.* B **1** 71
[106] Edwards S F 1965 *Proc. Phys. Soc.* **85** 613
[107] Matsen M W and Bates F S 1996 *Macromolecules* **29** 1091
[108] Matsen M W 1999 *J. Chem. Phys.* **110** 4658
[109] Thompson R B and Matsen M W 2000 *J. Chem. Phys.* **112** 6863
[110] Thompson R B and Matsen M W 2000 *Phys. Rev. Lett.* **85** 670
[111] Kodama H, Komura S and Tamura K 2001 *Europhys. Lett.* **53** 46
[112] Komura S, Kodama H and Tamura K 2002 *J. Chem. Phys.* **117** 9903
[113] Düchs D, Ganesan V, Fredrickson G H and Schmid F 2003 *Macromolecules* **36** 9237
[114] Krishnan K, Almdal K, Burghardt W R, Lodge T P and Bates F S 2001 *Phys. Rev. Lett.* **87** 098301
[115] Caputo F E, Burghardt W R, Krishnan K, Bates F S and Lodge T P 2002 *Phys. Rev.* E **66** 041401
[116] Krishnan K, Burghardt W R, Lodge T P and Bates F S 2002 *Langmuir* **18** 9676
[117] Burghardt W R, Krishnan K, Bates F S and Lodge T P 2002 *Macromolecules* **35** 4210

[118] Narayanan B, Pryamitsyn V and Ganesan V 2006 *Phys. Rev. Lett.* **96** 028302
[119] Jakobs B, Sottmann T, Strey R, Allgaier J, Willner L and Richter D 1999 *Langmuir* **15** 6707
[120] Endo H, Allgaier J, Gompper G, Jakobs B, Monkenbusch M, Richter D, Sottmann T and Strey R 2000 *Phys. Rev. Lett.* **85** 102
[121] Endo H, Mihailescu M, Monkenbusch M, Allgaier J, Gompper G, Richter D, Jakobs B, Sottmann T, Strey R and Grillo I 2001 *J. Chem. Phys.* **115** 580
[122] Gompper G, Richter D and Strey R 2001 *J. Phys.: Condens. Matter* **13** 9055
[123] Gompper G, Endo H, Mihailescu M, Allgaier J, Monkenbusch M, Richter D, Jakobs B, Sottmann T and Strey R 2001 *Europhys. Lett.* **56** 683
[124] Hiergeist C and Lipowsky R 1996 *J. Physique* II **6** 1465
[125] Komura S and Safran S A 2001 *Eur. Phys. J.* E **5** 337
[126] Mihailescu M, Monkenbusch M, Endo H, Allgaier J, Gompper G, Stellbrink J, Richter D, Jakobs B, Sottmann T and Farago B 2001 *J. Chem. Phys.* **115** 9563
[127] Byelov D, Frielinghaus H, Holderer O, Allgaier J and Richter D 2004 *Langmuir* **20** 10433
[128] Holderer O, Frielinghaus H, Byelov D, Monkenbusch M, Allgaier J and Richter D 2005 *J. Chem. Phys.* **122** 094908
[129] Monkenbusch M, Holderer O, Frielinghaus H, Byelov D, Allgaier J and Richter D 2005 *J. Phys.: Condens. Matter* **17** S2903
[130] Nakaya K, Imai M, Komura S, Kawakatsu T and Urakami N 2005 *Europhys. Lett.* **71** 494
[131] Filali M, Ouazzani M J, Michel E, Aznar R, Porte G and Appell J 2001 *J. Phys. Chem.* B **105** 10528
[132] Zilman A, Kieffer J, Molino F, Porte G and Safran S A 2003 *Phys. Rev. Lett.* **91** 015901
[133] Hed G and Safran S A 2006 *Eur. Phys. J.* E **19** 69
[134] Lusvardi K M, Schubert K V and Kaler E W 1996 *Ber. Bunsenges. Phys. Chem.* **100** 373
[135] Ganesan V and Fredrickson G H 2000 *J. Phys. Chem.* **113** 2901